

Article

Erosion Layer Growth between Solid 316L Stainless Steel and Al–Li Alloy Melt

Zhanwei He, Xiaojun Hu *, Wan Han, Xudong Mao and Kuo-Chih Chou

The State Key Laboratory of Advanced Metallurgy, University of Science and Technology Beijing, Beijing 100083, China; hezhanwei@ustb.edu.cn (Z.H.); g20209302@xs.ustb.edu.cn (W.H.); maoxudong@xs.ustb.edu.cn (X.M.); kcc126@126.com (K.-C.C.)

* Correspondence: huxiaojun@ustb.edu.cn

Abstract: The erosion experiments of Al–Li melt on 316L stainless steel were carried out at different temperatures and holding times. In this study, the microstructure and composition of an Al–Li/316L liquid–solid interface was analyzed by inductively coupled plasma atomic emission spectrometer (ICP-AES), scanning electron microscopy (SEM), and energy dispersive spectroscopy (EDS). The phase transformation and structure evolution of the erosion process were studied to explain the erosion mechanism and kinetics. The results showed that Fe/Cr/Ni–Al intermetallic compounds (IMC) were formed at the Al–Li/316L interface, and the diffusion of Cr atoms lead to the accumulation of Ti in the Al–Li melt, to form $TiAl_3$ and $CrAl_4$. With the increase in temperature and holding time, the thickness of the Fe-containing erosion layer (EL) increased, and the morphology of Ti-containing erosion particles (EP) became larger and more regular. The apparent activation energy (E_a) of the Fe-containing erosion layer was $124.82\text{ kJ}\cdot\text{mol}^{-1}$. Meanwhile, a kinetics equation for predicting the service life of 316L was obtained. The research results provided a theoretical guidance for the smelting and casting of an Al–Li alloy.



Citation: He, Z.; Hu, X.; Han, W.; Mao, X.; Chou, K.-C. Erosion Layer Growth between Solid 316L Stainless Steel and Al–Li Alloy Melt. *Metals* **2022**, *12*, 350. <https://doi.org/10.3390/met12020350>

Academic Editors: Junsheng Wang and Wislei Riuper Osório

Received: 31 December 2021

Accepted: 8 February 2022

Published: 17 February 2022

Publisher's Note: MDPI stays neutral with regard to jurisdictional claims in published maps and institutional affiliations.



Copyright: © 2022 by the authors. Licensee MDPI, Basel, Switzerland. This article is an open access article distributed under the terms and conditions of the Creative Commons Attribution (CC BY) license (<https://creativecommons.org/licenses/by/4.0/>).

Keywords: Al–Li; 316L; erosion; kinetics; phase transformation

1. Introduction

As an emerging lightweight alloy, the Al–Li alloy provides an opportunity to significantly improve the performance of aerospace components, due to its low density and good corrosion resistance [1–3]. The use of the Al–Li alloy to manufacture aircraft components can reduce the weight of the aircraft by 10~20%, thereby reducing costs and improving the carrying capacity of the aircraft. Therefore, Al–Li alloys have become the focus of research in recent years [4–6].

Previous studies have shown that the properties of Al alloys are closely related to element content [7–10], so the addition of Li greatly changed the performance of the Al alloy. Due to the addition of Li [11,12], the density can be reduced, Young's modulus of elasticity, fatigue crack growth resistance and corrosion resistance can be improved, but there will be problems, such as easier oxidation of the melt and more difficult casting and smelting. At present, Fe-based alloys, such as stainless steel, are widely used in the smelting and casting of Al alloys, but molten Al–Li alloys at high temperatures have strong chemical activity and will corrode the stainless steel used as casting materials. Stainless steel, as a multi-metallic Fe-based alloy, is corroded by Al–Li alloys to form a variety of complex intermetallic compounds, which are also studied by relevant researchers [13–16]. Bouche [17] studied the intermetallic compound layer at the Al/Fe liquid–solid interface and explained its growth mechanism. Jindal [18] studied the diffusion behavior of the Al/Fe solid–solid diffusion couple at 500~600 °C. Jiang [19,20] investigated the phase transition and growth mechanism of intermetallic compounds at the Al/Ti and Al/Ni liquid–solid interface, respectively. However, their research mainly focused on the erosion between pure metal Al and Fe/Ti/Ni, which could not fully reflect its erosion behavior on

Fe-based alloys. Besides, Wang [21] proposed that increasing the content of Li in the Al-Li melt can aggravate the corrosion of TC4 titanium alloys by Al. Therefore, it is necessary to study the erosion behavior of Al-Li alloys on Fe-based alloys.

In this study, 316L was selected as an Fe-based alloy with good heat resistance. The phase transformation and structure evolution of the erosion layer at the Al-Li/316L liquid-solid interface was analyzed under different temperatures and holding times. The erosion behavior of the Al-Li alloy melt, coexisting with various elements in 316L, was studied. Meanwhile, the erosion kinetic equation was established, and the service life of 316L as a casting material was predicted. The research results will improve the erosion theory of Al-Li alloys on Fe-based alloys and provide guidance for the protection of 316L with coating.

2. Experimental

2.1. Material Preparation

The prepared Al-Li alloy ingot and 316L were used as raw materials. The Al-Li alloy was cut from ingot into a $\Phi 19(\pm 0.2)$ mm* $30(\pm 0.5)$ mm bar as the outer matrix material, and 316L was cut into a block with a size of $5(\pm 0.1)$ mm* $5(\pm 0.1)$ mm* $50(\pm 0.5)$ mm. The chemical composition of Al-Li alloy and 316L was determined by ICP-AES, as shown in Table 1. Al-Li alloy was cleaned with 5% NaOH solution for 5 min to remove the oxide film before melting. To make Al-Li alloy melt and 316L have a better interface, 316L was polished with sandpaper (120#, 400#, 600#, 800#, 1000#, 1500#, 2000#) and polishing paste to remove the oxide film and make the surface smoother.

Table 1. Chemical composition of Al-Li alloy and 316L (wt %).

Sample	Al	Li		Cu		Ti	Zn	Mg	
Al-Li	91.59	2.34		4.67		0.07	0.77	0.56	
Sample	Fe	Cr	Ni	Mo	Mn	Ti	Si	S	C
316L	68.75	17.28	10.62	1.94	1.30	<0.01	0.11	<0.01	0.03

2.2. Procedures

The experiment was carried out in a high-temperature tube furnace as shown in Figure 1a. Considering the melting point and casting process of Al-Li alloy, 680 °C, 700 °C, 720 °C were determined as the target temperature of the experiment. When the tube furnace was heated to the target temperature (680, 700, 720 °C), Al-Li alloy bar was placed in the crucible of the constant temperature zone in the furnace. The Al-Li alloy was heated for 20min at 300mL/min Ar, at which time the Al-Li alloy had completely melted. Subsequently, 316L was rapidly inserted into the Al-Li alloy melt, kept warm at the Ar atmosphere and the target temperature, and the timing was started. Figure 1b shows the size of the crucible and the detailed process of the experiment. First, the crucible was taken out after 10, 20, 30, 60, and 90 min, successively, and cooled to room temperature. During the heat preservation and cooling process, Ar protection with a flow rate of 300 mL/min was always carried out. Second, the cooled Al-Li alloy block was taken out from the crucible and cut along the dotted line, as in Figure 1b. Finally, the samples obtained by wire cutting were polished for microstructure observation.

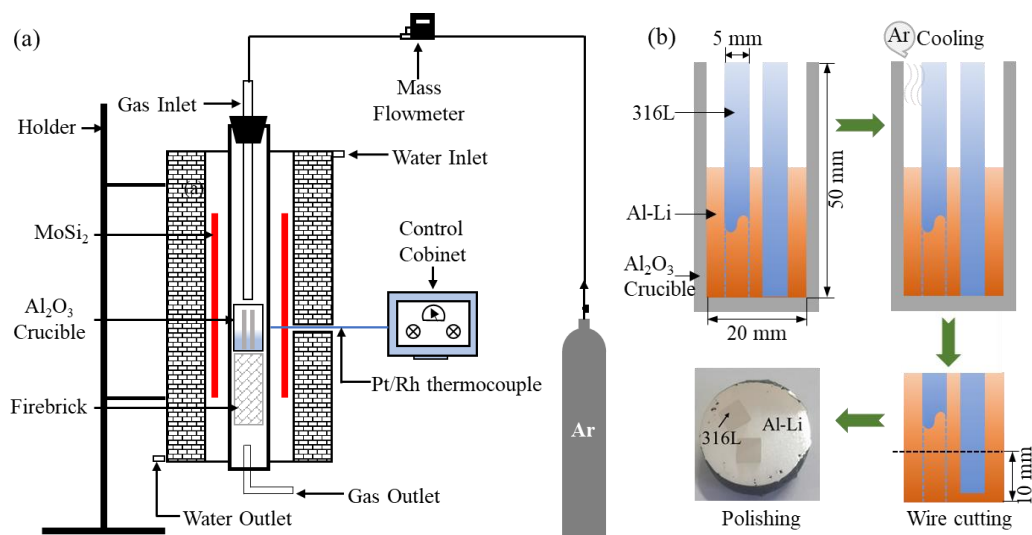


Figure 1. Schematic diagram of the experimental device and process (a) Tube furnace; (b) Crucible size and experimental process.

The morphology of microstructure and elemental content in the Al–Li/316L interface was characterized by using a scanning electron microscope (SEM, ZEISS, Germany) with an energy dispersive spectroscopy. The erosion interface with flat and uniform thickness of the erosion layer should be selected for observation and analysis. In order to reduce the error of the experimental data, the thickness of the erosion layer under different fields of view was measured and recorded on the same sample. Meanwhile, the measured data were processed and analyzed to obtain the growth kinetic equation of the erosion layer.

3. Results and Discussion

3.1. Microstructure and Composition of Erosion Layer

Figure 2 is the area scanning image of the Al–Li/316L liquid–solid interface after holding at 720 °C for 20 min, and 90 min by SEM. The right side of the SEM image is the solidified structure of the Al–Li alloy, and the left side is the 316L. As shown in Figure 2a, there are two obvious erosion layers between them, mainly including the massive EP2 in the Al–Li alloy and EL1 near the interface, which is composed of a dense solid layer near 316L, and a strip structure near the Al–Li alloy. The distribution of corresponding elements is represented by different colors and levels of brightness. It can be seen that FeAl₃ mainly contains Al, Fe, and Cr elements, while the EP2 is composed of Al, Cr, and Ti elements. As the holding time increases to 90 min, the EL1 becomes thicker. At the same time, a denser EL3 was observed between 316L and EL1, as shown in the red dashed area in Figure 2b. By observing the brightness of the corresponding color of the elements in the red dashed area, it can be seen that it is mainly composed of Al, Fe, Cr, and Ni elements. The brightness contrast with the corresponding colors of the elements in the EL1 and EL3 also shows that both erosional layers are composed of an Fe-containing erosion product, but their element content is slightly different. For simplicity, the Fe-containing erosion layer is analyzed as a whole in subsequent kinetics analysis, including the EL1 and EL3 in Figure 2b. However, the constituent elements of EP2 are the same as those at 20 min, except that its appearance is more regular.

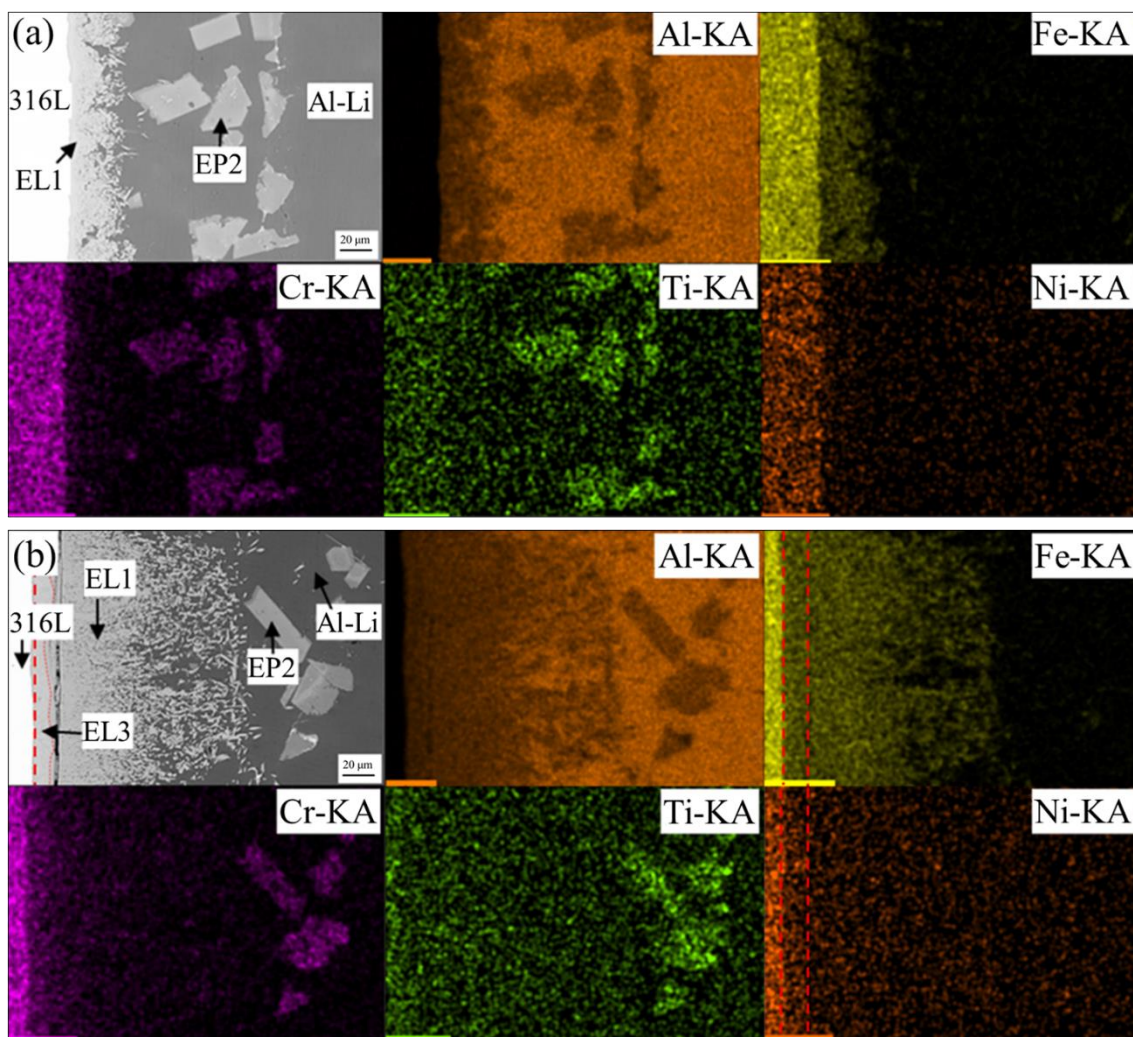


Figure 2. Element distribution on the Al-Li/316L interface at 720 °C for 20 min and 90 min **(a)** 20 min; **(b)** 90 min.

The EDS analysis was performed to identify the phase composition of EL1, EP2, and EL3 in Figure 2a,b, and the results are listed in Table 2. Combined with the Al–Fe/Cr/Ti/Ni binary phase diagram (Figure 3), the phase composition of the EL1, EP2, and EL3 can be inferred.

Table 2. EDS (energy dispersive spectroscopy) analysis of the results in Figure 2 (at%).

Layer	Al	Fe	Cr	Ti	Ni
Figure 2a (20 min)	EL 1	81.07	14.78	4.15	-
	EP 2	91.32	-	6.09	2.59
Figure 2b (90 min)	EL 1	81.29	14.59	4.12	-
	EP 2	91.68	-	6.05	2.27
	EL 3	72.57	20.55	4.81	2.07

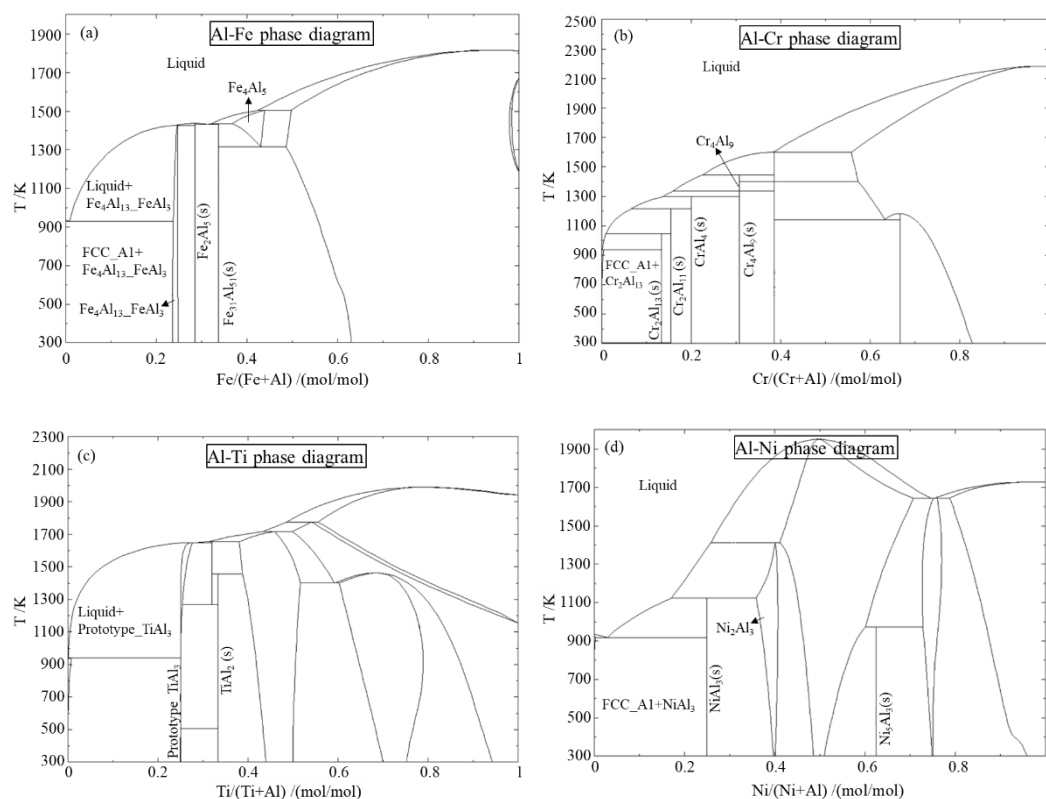


Figure 3. Al–Fe/Cr/Ti/Ni binary phase diagram **(a)** Al–Fe; **(b)** Al–Cr; **(c)** Al–Ti; **(d)** Al–Ni.

As can be seen from Figure 2, the erosion of 316L by the Al–Li alloy melt is mainly the reaction of Al with Fe, Ni, Cr, and Ti. The binary phase diagrams of Al–Fe/Cr/Ti/Ni were plotted using the FactSage software package (FactSage 7.0, Thermfact and GTT Technologies, Montreal Canada and Aachen Germany). It can be seen from Figure 2 that the EL1 is close to the Al–Li alloy, and Fe, Cr content is relatively small. According to the atomic ratio of EDS in Table 2 and the Al–Fe/Cr binary phase diagrams in Figure 3, it can be seen that the EL1 is composed of FeAl₃ and Cr₂Al₁₃. Similarly, the EL3 is near 316L, so the EL3 is composed of Fe₂Al₅, CrAl₄, Ni₂Al₃. The EP2, containing Cr and Ti, is in the Al–Li melt, and the content of Cr and Ti is relatively small. According to Figure 3b,c, the intermetallic compounds formed are Cr₂Al₁₃ and TiAl₃.

3.2. Formation Mechanism of Fe-Containing Erosion Layer

Figure 4 shows the microstructures of the Al–Li/316L liquid–solid interface, after holding at 720 °C for 10 min, 20 min, 30 min, 60 min, respectively. With the increase in holding time, the thickness of the EL1 increases gradually. The formation mechanism of the Al–Li/316L liquid–solid interface erosion layer, by analyzing its phase and the evolution process of its organizational structure, is shown in Figure 5.

At the initial stage of heat preservation (Figure 5a), under the action of the concentration gradient at the Al–Li/316L liquid–solid interface, Al atoms of Al–Li melt and Fe atoms of 316L diffuse to each other, but it is mainly based on the diffusion of Fe atoms in the 316L into the Al–Li melt. Subsequently (Figure 5b), when Fe atoms reach saturation in the Al–Li melt at the interface, a chemical reaction occurs to form intermetallic compounds. At this time, Fe is in the Al-rich region, and it can be seen from Figure 3a that FeAl₃ is formed. A steady stream of Fe atoms diffuses into the Al–Li melt to generate a large number of FeAl₃ and gather near the interface. This process is dominated by chemical reactions, so an obvious erosion layer appears in a short time. In Figure 4, the thickness of the EL1 after 10 min reached 31.3 μm. This could also explain why there is little difference in the thickness of the EL1 at 10 min and 20 min.

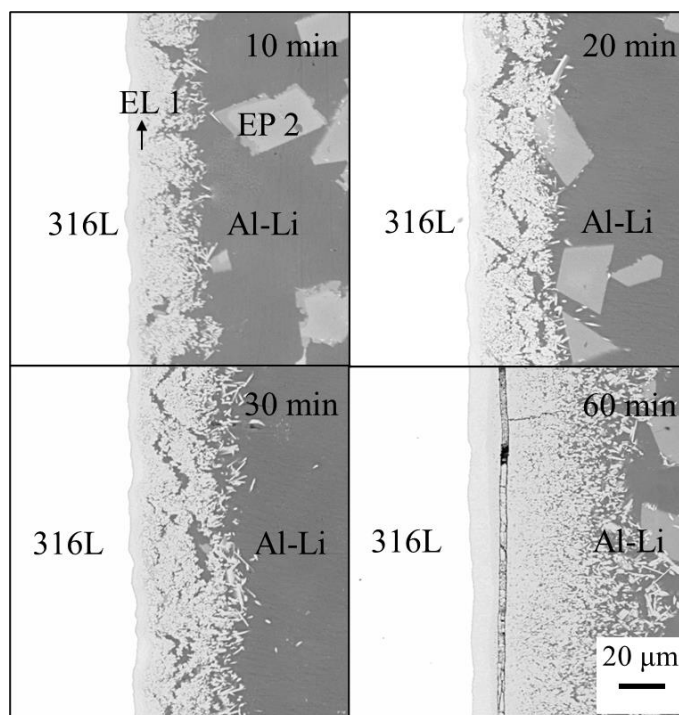


Figure 4. Influence of holding time on the microstructure of EL1 at 720 °C.

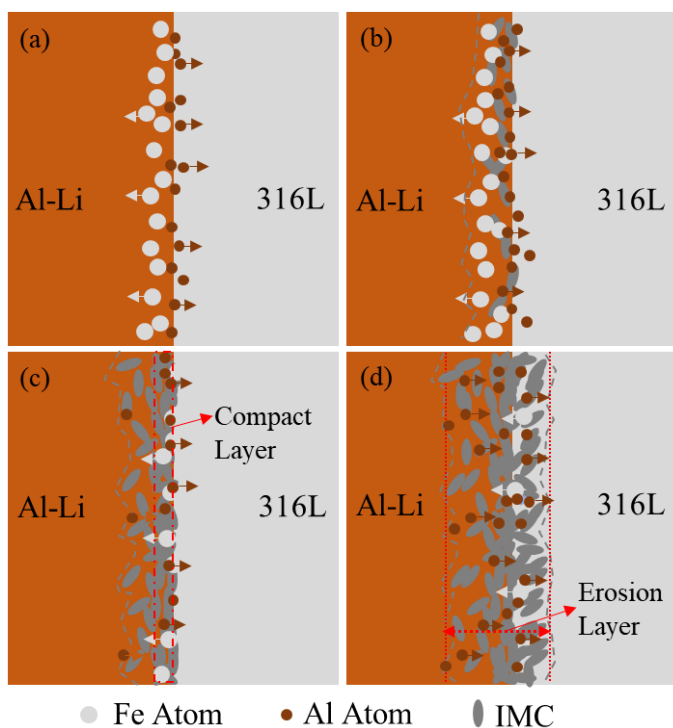


Figure 5. Evolution process of organizational structure (a) at the initial stage; (b) Initial reaction stage; (c) Midterm reaction stage; (d) Later reaction stage.

As the holding time increases (Figure 5c), the intermetallic compounds preferentially grow laterally along the interface. When a dense layer is formed, the contact between the Al-Li melt and 316L is blocked, so that the diffusion becomes dominated by the diffusion of Al in the FeAl_3 . At the later stage of heat preservation (Figure 5d), Al atoms diffuse through the FeAl_3 layer and reach the IMC/316L interface. At this point, Fe at the solid-solid interface is in the Al-poor zone and continues to react to form Fe_2Al_5 . However, the

continued diffusion of Al will dissolve Fe_2Al_5 , so there is little difference in the thickness of the EL3 between 60 min and 90 min. In the above two stages, diffusion is the restrictive link, so that the amount of erosion produced is limited and will not cause a sharp increase in the thickness of the erosion layer. Therefore, the thickness of the Fe-containing erosion layer increases with the holding time.

Five SEM images of the interface between the Al–Li alloy and 316L, at various temperatures and holding times, were randomly selected. The microstructure of SEM images was analyzed and the thickness of the erosion layer was measured, respectively. The mean value of the measurement results is the thickness of the eroded layer, which is listed in Table 3. The SEM images, at various temperatures and holding times, were randomly selected as representatives, and their microstructures are shown in Figure 6. It can be seen that the thickness of the Fe-containing erosion layer not only changes with the change of holding time, but also changes with the change of temperature. As the temperature increases, the thickness of the EL1 under the same holding time increases. Furthermore, there is a difference in the thickness of the EL1 between different temperature increases with holding time. When the holding time is increased to 90 min, the temperature increases and the thickness of the EL1 increases. Therefore, the thickness of the EL1 is also closely related to temperature.

Table 3. Thickness of EL1 at different temperatures and holding times.

T/°C	d/ μm			
	20 min	30 min	60 min	90 min
680	21.60	26.70	44.43	61.87
700	30.18	39.55	62.98	86.36
720	40.23	52.05	84.66	114.89

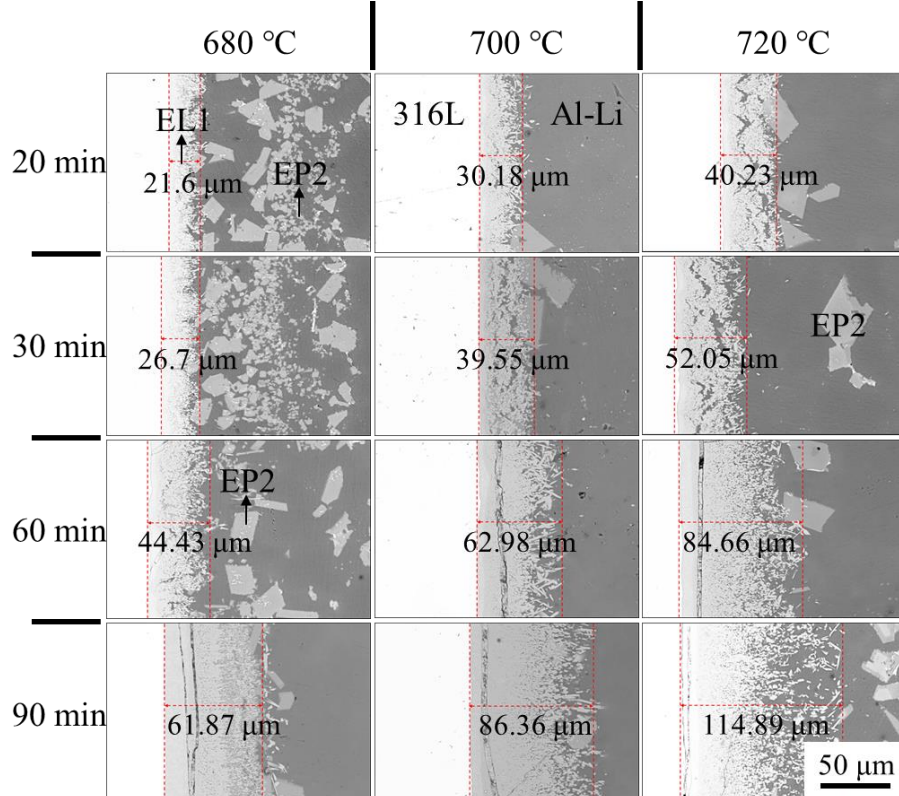


Figure 6. Morphology of EL1 and EP2 at different temperatures and holding time.

The above analysis shows that the Fe-containing erosion layer mainly comes from the diffusion erosion of the Al–Li alloy to 316L, so the thickness of the erosion layer (EL1) is closely related to the holding time and temperature, as shown in Equation (1) [20].

$$d(T) = K(T)(t)^n \quad (1)$$

Here, d represents the thickness of the erosion layer, mm; K is the growth coefficient of the erosion layer; n is the growth index; t is the holding time. Take the logarithm of Equation (1), as follows:

$$\ln d = \ln K + n \ln t \quad (2)$$

The data in Table 3 were substituted into Equation (2) to plot the relationship between $\ln d$ and $\ln t$, as shown in Figure 7. The values of n and K were calculated by linear fitting and are listed in Table 4.

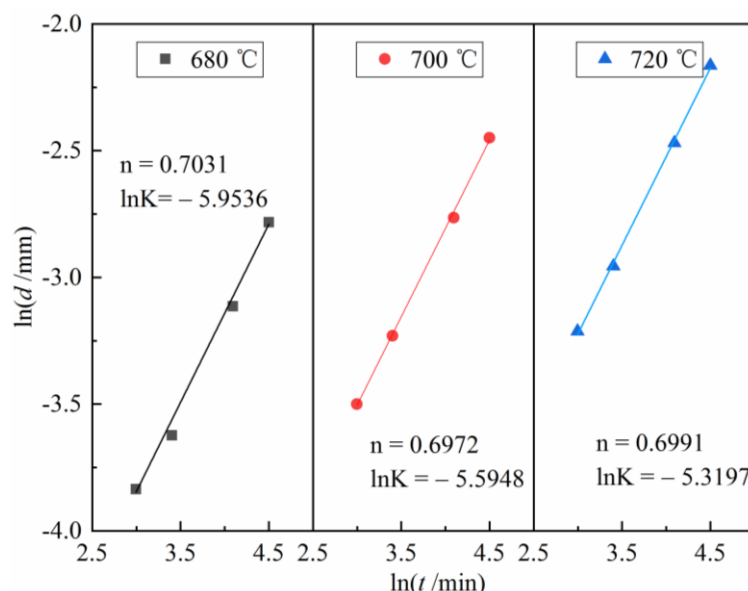


Figure 7. Relationship between $\ln d$ and $\ln t$ at different temperatures.

Table 4. Growth coefficient (K) and growth index (n) at different temperatures.

Temperature T/K	Growth Coefficient K	Growth Index n
680	0.002596	0.7031
700	0.003717	0.6972
720	0.004894	0.6991

In Table 4, the growth index n is about 0.7, which can be interpreted as the reaction rate, controlled by both diffusion and chemical reaction. The growth coefficient (K) of the erosion layer increased with temperature, indicating that higher temperatures would aggravate the erosion of the Al–Li alloy on 316L and shorten its service life. K is related to the reaction temperature T , which can be expressed by the Arrhenius equation, as follows:

$$K(T) = A \exp\left(\frac{-E_a}{RT}\right) \quad (3)$$

$$\ln K(T) = \ln A - \frac{E_a}{RT} \quad (4)$$

where A is the pre-exponential factor; E_a is the apparent activation energy, kJ/mol; R is the gas constant, $8.314 \text{ J} \cdot \text{mol}^{-1} \cdot \text{K}^{-1}$.

According to the data in Table 4, the relationship between $\ln K(T)$ and $1/T$ is drawn, as shown in Figure 8. The apparent activation energy E_a was calculated by a linear fitting

slope, and the value of E_a was $124.82 \text{ kJ}\cdot\text{mol}^{-1}$. Based on the above analysis and calculation data, the growth kinetic equation of the Al–Li/316L liquid–solid interface erosion layer can be established and shown in Equation (5), so as to calculate the service life of 316L as casting material.

$$d = 1.819 \times 10^4 \exp\left(\frac{1.2482 \times 10^5}{RT}\right) t^{0.6998} \quad (5)$$

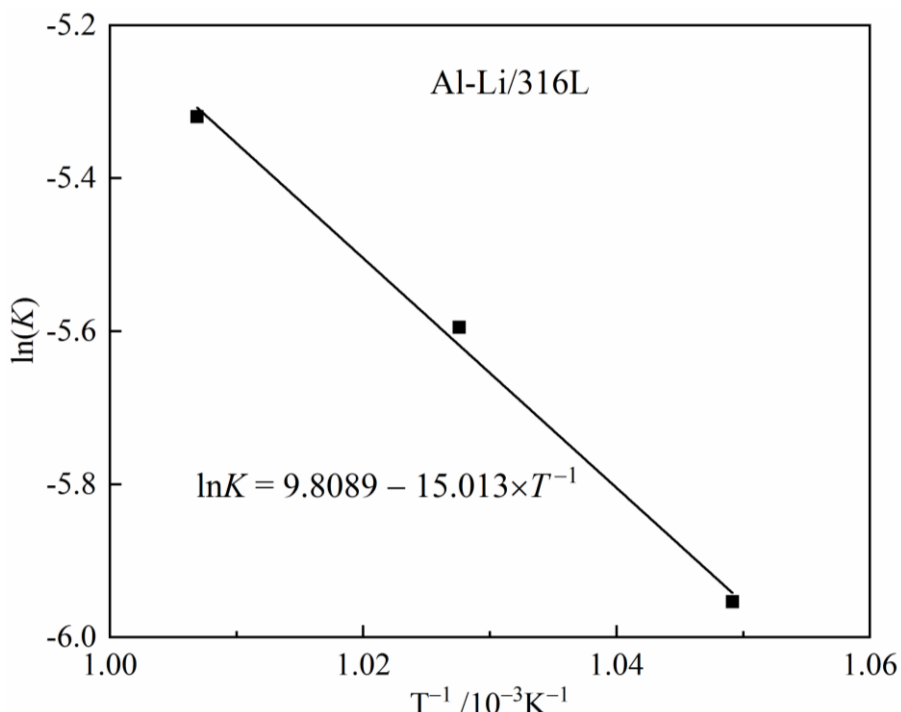


Figure 8. Arrhenius plot for the evaluation of the activation energy of the process.

The formation mechanism of the Al–Cr IMC in the EL1 is similar to that of Al–Fe IMC. During the heat preservation process, $\text{Cr}_2\text{Al}_{13}$ is mainly formed, and as the holding time increases, it becomes CrAl_4 at the solid–solid interface. The Ni-containing erosion layer near 316L is mainly composed of Ni_2Al_3 .

3.3. Formation Mechanism of Cr/Ti Erosion Layer

In Figure 6, the EP2 in the Al–Li melt is mainly composed of $\text{Cr}_2\text{Al}_{13}$ and TiAl_3 . It can be seen from Table 1 that the Ti content in 316L is much lower than in the Al–Li alloy, so Ti in TiAl_3 mainly comes from the Al–Li melt. The Al–Li alloy, without 316L, was kept at the target temperature for 90 min, with no aggregation of Ti and no formation of Ti-containing IMC. When 316L was inserted into the Al–Li alloy melt, the Cr atoms diffused into the Al–Li melt, and Ti aggregated and formed TiAl_3 at the same time. This kind of erosion not only changes the chemical composition of the Al–Li alloy, but also produces impurities, thus, causing pollution to the Al–Li alloy.

At the initial stage of heat preservation, Cr atoms in 316L diffuse into the Al–Li melt, which not only forms $\text{Cr}_2\text{Al}_{13}$, but also leads to the aggregation of Ti to form TiAl_3 . With the increase in holding time, the dense FeAl_3 layer also prevents the diffusion of Cr into the Al–Li melt, so EP2 exists in the Al–Li melt. In Figure 6, when holding at 680°C for 20 min, EP2 was blocky and granular, small in size. With the increase in holding time, the particles gathered and gradually disappeared, while the blocky size also increased significantly. At 700°C and 720°C , EP2 is mainly composed of regular blocky IMC.

4. Conclusions

Based on the erosion experiment of the Al–Li alloy on 316L, at different temperatures and holding times, the reaction kinetics, phase transformation, and structure evolution processes in the erosion process were systematically investigated to achieve the prediction of the service life of 316L.

(1) At different temperatures and holding times, the erosion layer mainly includes an Fe/Cr/Ni-containing erosion layer near 316L and Cr/Ti-containing erosion layer in the Al–Li alloy melt. With the increase in holding time, the composition of the Fe-containing erosion layer changed (from FeAl_3 , $\text{Cr}_2\text{Al}_{13}$ to FeAl_3 , Fe_2Al_5 , $\text{Cr}_2\text{Al}_{13}$, CrAl_4 , and Ni_2Al_3) but the composition of the Cr/Ti-containing erosion layer did not change ($\text{Cr}_2\text{Al}_{13}$ and TiAl_3).

(2) The thickness of the Fe-containing erosion layer (EL1) is closely related to temperature and holding time. With the increase in temperature and holding time, the EL1 thickness gradually increased. The E_a value for the erosion process was calculated to be $124.82 \text{ kJ}\cdot\text{mol}^{-1}$, and the thickness of the erosion layer equation was $d = 1.819 \times 10^4 \exp\left(\frac{-1.2482 \times 10^5}{RT}\right) t^{0.6998}$.

(3) The Cr/Ti-containing erosion layer (EP2) is formed in a short time and is closely related to the diffusion of Cr atoms in the Al–Li melt. As the holding time and temperature increase, EP2 is always in the Al–Li melt, and the particle size increases. This erosion can contaminate the Al–Li alloy.

Author Contributions: Conceptualization, X.H., K.-C.C. and Z.H.; methodology, X.H. and Z.H.; validation, X.H. and Z.H.; formal analysis, Z.H. and X.M.; investigation, Z.H. and W.H.; data curation, Z.H.; writing-original draft preparation, Z.H.; writing-review and editing, Z.H.; supervision, X.H. and K.-C.C.; project administration, X.H.; funding acquisition, X.H. All authors have read and agreed to the published version of the manuscript.

Funding: The author is thankful for the financial support from the State Key Laboratory of Advanced Metallurgy (Grant No. 41621025, Thermodynamic and Kinetic Research on Casting Process of Al–Li Alloy System).

Institutional Review Board Statement: No applicable.

Informed Consent Statement: Not applicable.

Data Availability Statement: Not applicable.

Conflicts of Interest: The authors declare no conflict of interest.

References

1. Kim, N.J.; Lee, E.W. Effect of T1 precipitate on the anisotropy of Al–Li alloy 2090. *Acta Metall. Mater.* **1993**, *41*, 941–948. [[CrossRef](#)]
2. Rioja, R.J. Fabrication methods to manufacture isotropic Al–Li alloys and products for space and aerospace applications. *Mater. Sci. Eng. A* **1998**, *257*, 100–107. [[CrossRef](#)]
3. Su, J.X.; Zhang, Z.; Cao, F.H.; Zhang, J.Q.; Cao, C.N. Exfoliation corrosion behavior of T6 treated 2090 Al–Li alloy in EXCO solution and EIS during exfoliation corrosion evolution. *Acta Metall. Sin.* **2005**, *41*, 974–978.
4. Xu, Y.B.; Zhong, W.L.; Chen, Y.J.; Shen, L.T.; Liu, Q.; Bai, Y.L.; Meyers, M.A. Shear localization and recrystallization in dynamic deformation of 8090 Al–Li alloy. *Mater. Sci. Eng. A* **2001**, *299*, 287–295. [[CrossRef](#)]
5. Lavernia, E.J.; Grant, N.J. Aluminum-lithium alloys. *J. Mater. Sci.* **1987**, *22*, 1521–1529. [[CrossRef](#)]
6. Du, Y.X.; Zhang, X.M.; Ye, L.Y.; Liu, S.D. Evolution of grain structure in AA2195 Al–Li alloy plate during recrystallization. *Trans. Nonferrous Met. Soc. China* **2006**, *16*, 321–326. [[CrossRef](#)]
7. Lloyd, D.J.; Court, S.A. Influence of grain size on tensile properties of Al–Mg alloys. *Mater. Sci. Technol.* **2003**, *19*, 1349–1354. [[CrossRef](#)]
8. Osório, W.R.; Cheung, N.; Spinelli, J.E.; Goulart, P.R.; Garcia, A. The effects of a eutectic modifier on microstructure and surface corrosion behavior of Al–Si hypoeutectic alloys. *J. Solid State Electrochem.* **2007**, *11*, 1421–1427. [[CrossRef](#)]
9. Bonatti, R.S.; Meyer, Y.A.; Bortolozo, A.D.; Costa, D.; Osório, W.R. Morphology and size effects on densification and mechanical behavior of sintered powders from Al–Si and Al–Cu casting alloys. *J. Alloys Compound.* **2019**, *786*, 717–732. [[CrossRef](#)]
10. Meyer, Y.A.; Bonatti, R.S.; Costa, D.; Bortolozo, A.D.; Osório, W.R. Compaction pressure and Si content effects on compressive strengths of Al–Si/Cu alloy composites. *Mater. Sci. Eng. A* **2020**, *770*, 138547. [[CrossRef](#)]
11. Rioja, R.J.; Liu, J. The evolution of Al–Li base products for aerospace and space applications. *Metall. Mater. Trans. A* **2012**, *43*, 3325–3337. [[CrossRef](#)]

12. Akhtar, N.; Akhtar, W.; Wu, S.J. Melting and casting of lithium containing aluminum alloys. *Int. J. Cast Met. Res.* **2015**, *28*, 1–8. [[CrossRef](#)]
13. Liu, L.H.; Che, C.S.; Kong, G.; Lu, J.T.; Zhang, S.H. Destabilization mechanism of Fe-Al inhibition layer in Zn-0.2% Al hot-dip galvanizing coating and related thermodynamic evaluation. *Acta Metall. Sin.* **2016**, *52*, 614–624.
14. Kattner, U.R.; Lin, J.C.; Chang, Y.A. Thermodynamic assessment and calculation of the Ti-Al system. *Metall. Trans. A* **1992**, *23*, 2081–2090. [[CrossRef](#)]
15. Xu, L.; Cui, Y.Y.; Hao, Y.L.; Yang, R. Growth of intermetallic layer in multi-laminated Ti/Al diffusion couples. *Mater. Sci. Eng. A* **2006**, *435*, 638–647. [[CrossRef](#)]
16. Zhang, L.J.; Wang, J.; Du, Y.; Hu, R.X.; Nash, P.; Lu, X.G.; Jiang, C. Thermodynamic properties of the Al-Fe-Ni system acquired via a hybrid approach combining calorimetry, first-principles and CALPHAD. *Acta Mater.* **2009**, *57*, 5324–5341. [[CrossRef](#)]
17. Bouche, K.; Barbier, F.; Coulet, A. Intermetallic compound layer growth between solid iron and molten aluminum. *Mater. Sci. Eng. A* **1998**, *249*, 167–175. [[CrossRef](#)]
18. Jindal, V.; Srivastava, V.C.; Das, A.; Ghosh, R.N. Reactive diffusion in the roll bonded iron-aluminum system. *Mater. Lett.* **2006**, *60*, 1758–1761. [[CrossRef](#)]
19. Jiang, S.Y.; Li, S.C.; Zhang, L. Microstructure evolution of Al-Ti liquid–solid interface. *Trans. Nonferrous Met. Soc. China* **2013**, *23*, 3545–3552. [[CrossRef](#)]
20. Jiang, S.Y.; Li, S.C. Formation mechanism and prediction of new phases in binary metallic liquid/solid interface. *Rare Met.* **2011**, *30*, 486–491. [[CrossRef](#)]
21. Wang, F.Y.; Wang, X.J.; Yan, Q.; Cui, J.Z. Corrosion behavior of TC4 titanium alloys in Al-Li alloy melt. *Metals* **2021**, *11*, 794. [[CrossRef](#)]